Research paper

Reservoir origin and characterization of gas pools in intrusive rocks of the Yingcheng Formation, Songliao Basin, NE China

Huafeng Tang [a,*], Xinying Zhao [a], Mingli Shao [b], Xianda Sun [c], Yan Zhang [a], Phiri Cryton [a]

[a] College of Earth Sciences, Jilin University, Changchun, Jilin 130061, China
[b] Petrochina Jilin Oilfield E&P Research Institute, Songyuan, Jilin 138000, China
[c] Petrochina Daqeld Oilfeld E&P Research Institute, Daqing, Heilongjiang 163001, China

ABSTRACT

In 2013, the first discovery of gas pools in well LS 208 in intrusive rocks of the Songliao Basin (SB), NE China was made in the 2nd member of the Yingcheng Formation in the Yingtai rift depression, proving that intrusive rocks of the SB have the potential for gas exploration. However, the mechanisms behind the origin of reservoirs in intrusive rocks need to be identified for effective gas exploration. The gas pool in intrusive rocks can be characterized as a low-abundance, high-temperature, normal-pressure, methane-rich, and lithologic pool based on integrated coring, logging, seismic, and oil test methods. The intrusive rocks show primary and secondary porosities, such as shrinkage fractures (SF), spongy pores (SP), secondary sieve pores (SSP), and tectonic fractures (TF). The reservoir is of the fracture–pore type with low porosity and permeability. A capillary pressure curve for mercury intrusion indicates small pore-throat size, negative skewness, medium–high displacement pressure, and middle–low mercury saturation. The development of fractures was found to be related to the quenching effects of emplacement and tectonic inversion during the middle–late Campanian. SP and SSP formed during two phases. The first phase occurred during emplacement of the intrusive rock in the late Albian, when the intrusions underwent alteration by organic acids. The second phase occurred between the early Cenomanian and middle Campanian, when the intrusions underwent alteration by carbonic acid. The SF formed prior to oil charging, the SSP + SP formed during oil charging, and the TF formed during the middle–late Campanian and promoted the distribution of gas pools throughout the reservoir. The intrusive rocks in the SB and the adjacent basins were emplaced in the mudstone and coal units, and have great potential for gas exploration.

© 2017 Elsevier Ltd. All rights reserved.

1. Introduction

Proven gas reserves occurring mainly in volcanic (~90%) and conglomeratic rock reservoirs of the Early Cretaceous Yingcheng Formation in the Songliao Basin of North-East China have exceeded 600×10^9 m^3 since 2002 (Feng, 2008; Liu et al., 2010a,b). The Yingcheng Formation is host to voluminous volcanic and associated intrusive and sedimentary rocks (Wang et al., 2007). The intrusive rocks contain primary and secondary fractures and solution caves (Gu et al., 2002; Wu et al., 2006; Sruoga et al., 2004) that have been crucial in the explorations of oil and gas in the Liaohe Basin (Wu et al., 2003; Gao et al., 2007), the shelf basin of the northeastern

China Sea (Cukur et al., 2010; Guo et al., 2013) and the Neuquén Basin of Northern Patagonia in Argentina (Rodriguez et al., 2009; Sruoga and Rubinstein, 2007).

In 2013, gas pools in gabbro-porphyrite rocks were first found in well LS208 at a depth of 4360–4480 m in the 2nd member of the Yingcheng Formation (Fig. 3). This proved that the intrusive rocks of the Songliao Basin have the potential for gas exploration. The tested gas segment lies between 4445 and 4452 m depths, and gas productivity is approximately 44.63×10^3 m^3/d, with CH$_4$ contents of 91.7%–93.67% (Table 1).

However, the origin and characteristics of these intrusive rock reservoirs is still poorly understood, and the mechanisms behind the accumulations of gas pools in these intrusive rock reservoirs will be of great importance in guiding further gas exploration in the basin.

The main objective of this study is to determine the reservoir

Table 1
The composition of the gas pool of intrusive rocks of the 2nd member of the Yingcheng Formation (K_1y^2) from well LS208 in the Yingtai rift depression in the Songliao basin, NE China.

Well	Depth(m)	NO.	Sample date	Relative density	Composition of gas (%)										
					CH_4	CH_6	C_3H_8	C_4H_{10}	C_4H_{10}	C_5H_{12}	C_5H_{12}	C_6H_{14}	O_2	N_2	CO_2
LS208	4452–4445	1	2013.10.8	0.5986	92.33	3.24	0.37	0.16	0.09	0	0	0	0.5	2.34	0.97
		2	2013.10.19	0.6003	91.04	3.22	0.42	0.14	0.08	0.02	0.01	0	0.93	4.03	0.1
		3	2013.10.8	0.5955	93.02	3.26	0.37	0.16	0.09	0	0	0	0.35	1.79	0.97
		4	2013.10.8	0.5927	93.67	3.29	0.38	0.16	0.09	0	0	0	0.2	1.24	0.98
		5	2013.9.8	0.5941	92.77	3.5	0.48	0.19	0.11	0.05	0	0	0.44	2.34	0.11

characteristics and origin of gas pools in the intrusive rocks in the Songliao Basin.

2. Geological setting

The tectonic evolution of the Meso–Cenozoic terrain in Songliao Basin of NE China comprises three main stages: (a) early synrift associated with the deposition of volcanogenic succession, (b) post-rift sag which favored the accumulations of sedimentary sequences, and (c) the depauperization period (a coarsening-upward sequence related to tectonic inversion) (Fig. 1). Approximately 45 rift depressions developed during these stages of rifting. The Yingtai Rift depression covers more than 1800 km^2 (695 mi^2) across the central–west part of the basin (Fig. 2a). The rift-related Cretaceous volcano-sedimentary succession of the Yingcheng Formation overlies Paleozoic metamorphic basement rocks and is widespread in other rift depressions of the Songliao Basin, forming a large igneous province (Cai et al., 2012; Jia et al., 2007; Wang et al., 2003) over an area of 0.85 × 10^6 km^2 (0.328 × 10^6 mi^2). The volcano-stratigraphy of the Yingcheng Formation is complex because of its lithology and stratigraphic texture (Tang et al., 2011, 2015; Wang et al., 2011a,b). The volcanic activity, which occurred over a time span of 25 Myr (135–110 Ma) in the Cretaceous (Wang et al., 1995), showed an eastward migration, reflecting tectonic changes during the different stages of collision between the Eurasian and Siberian plates. The emplacement of the Yingcheng Formation was coeval with regional lithospheric extension that began during the Jurassic (Yang et al., 2005). The rift system comprises inverted grabens, controlled by the NE-SW trending faults (Feng et al., 2010; Ge et al., 2012). The northern part of the Yingtai rift depression trends NNE-SSW, whereas the central-southern part trends NNW-SSE, and the rift depression was located in the west by the Wukeshu Fault. In the Late Aptian to Early Albian, the Yingtai Rift depression was inverted, leading to the greater uplift and denudation of the Yingcheng Formation (Fig. 2b).

The Yingtai Rift depression comprises 3 stratigraphic formations, namely, the Huoshiling, Shahezi, and Yingcheng Formations. However, unlike the Shahezi Formation, the Huoshiling Formation is not exposed. The Shahezi Formation comprises 3 stratigraphic members; the 1st and 3rd members mainly contain sandstones, while the 2nd member is predominantly mudstones. The Yingcheng Formation mainly comprises 2 stratigraphic members; the 1st member contains voluminous rhyolite with associated intermediate lavas and tuffs, and the 2nd member is mainly mudstone, along with intrusive rocks and sandstones (Fig. 2c).

3. Methods

We analyzed the reservoir characteristics of the 8.5-m drillcore samples of intrusive rocks from the 2nd member of the Yingcheng Formation using integrated coring, logging, seismic imagery, and oil testing. Void spaces are described using megascopic observations. Thin sections were impregnated with blue epoxy resin at a pressure

of 30 MPa over 30 h. The test temperature and humidity were 22.3 °C and 35% RH, respectively.

Whole-rock analyses were performed on three (3) fresh, unaltered gabbro–porphyrite and sub-alkaline volcanic rock samples. Major elemental compositions were determined with XRF using a D/MAX-2400 instrument manufactured by Rigaku Co, Ltd, in the Rock-Mineral Preparation and Analysis Lab at the Geology and Geophysics Research Institute of the Chinese Academy of Sciences, Beijing city, China. Ferroporphyrin and ignition loss were measured by volumetric and gravimetric methods, respectively.

Porosity and permeability tests were conducted jointly using the AP608 instrument at the Jilin University Rock Physics Lab (Changchun city, Jilin province, China) through helium (He) injection, based on the sample sizes listed in Table 2. The test temperature was 20 °C, and testing was performed according to the standard method of the Petroleum Industry of the People's Republic of China (SY/T 5336–2006, "Cores Analytical Method").

Capillary pressure measurements using the mercury intrusion method were conducted at the Fluid Mechanics Laboratory at the Daqing Oilfield Company E&D Research Institute using an AutoPore IV 9505 porosity analyzer. The test standard temperature and humidity were 18.6 °C and 40% RH, respectively. The test followed the standard method of the Petroleum Industry of the People's Republic of China (SY/T 5346–2005: "Capillary Pressure Curve Measurements of Rocks"). The imagery was captured with a Leica SP5 laser confocal scanning microscope (LCSM) at the Fluid Mechanics Laboratory, Daqing Oilfield Company E&D Research Institute, Daqing city, Hei Longjiang province, China.

We performed a burial history analysis from one denudation boundary in well LS208. The acoustic time method was used to calculate the denudation thickness between the boundaries of the Qingshankou and Sifangtai Formations. A burial curve was constructed based on stratum lithology and thickness, and on the increase in compression with burial depth.

The inclusion test was measured at the Analytical Laboratory of BRIUG in Beijing, using the LINKAM THMS600, and its cooling-heating stage which was produced by Linkam Scientific Instruments Ltd, UK. The test method was performed according to the EJ/T 1105–1999 standard method, at a test temperature of 26 °C and test air relative humidity of 40%.

4. Characteristic features of the intrusive rocks and gas pool

4.1. Intrusive rocks

The greenish gray gabbro–porphyrite and sub-alkaline intrusive rocks recorded a total thickness of 120 m. These rocks have hypocrystalline and ophitic textures, with irregular and columnar plagioclase, irregular and granular pyroxene, and opaque minerals (Fig. 4). Both the pyroxene and plagioclase underwent varying degrees of alteration, as evidenced by secondary clay minerals such as chlorite.
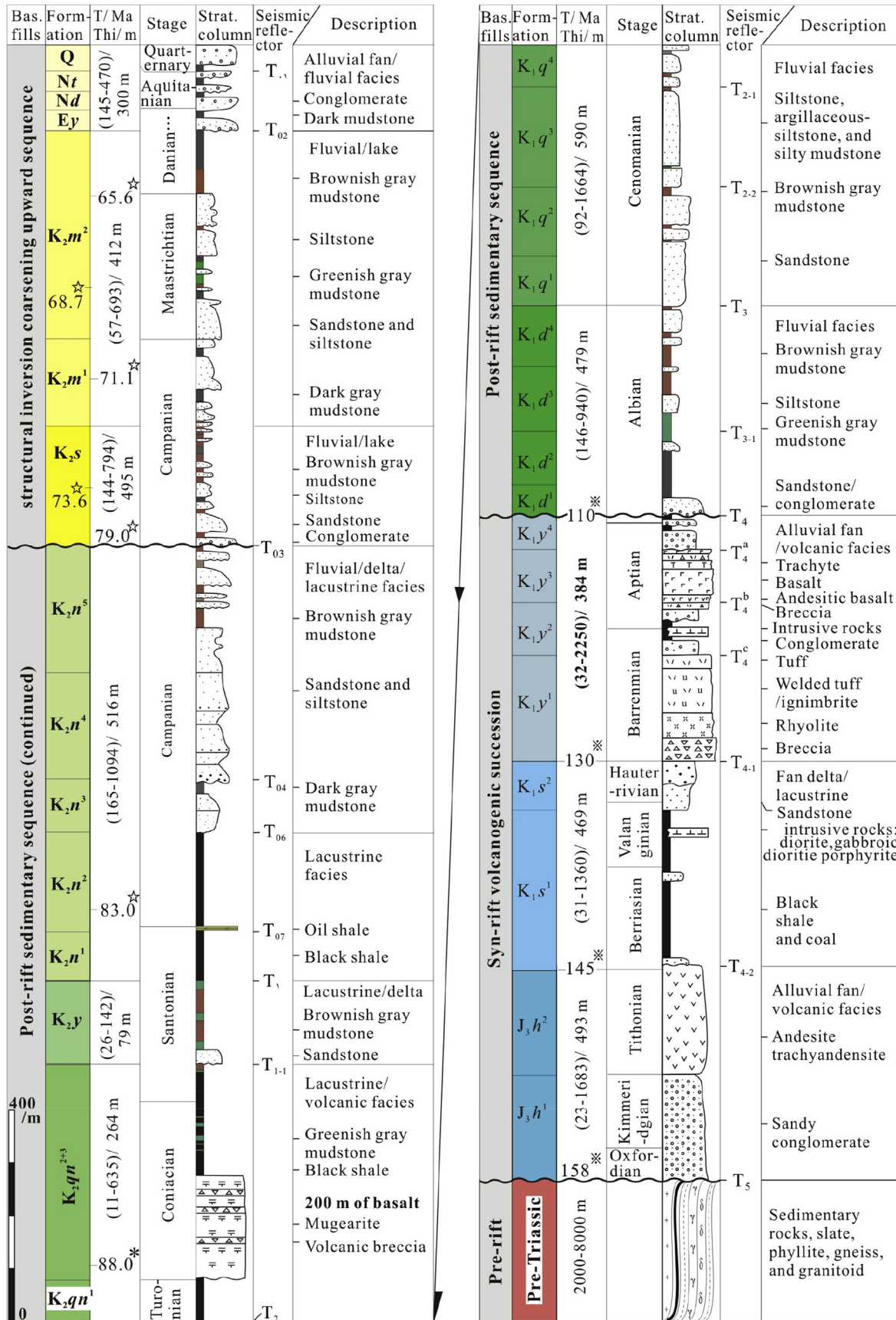
The gabbro–porphyrite is characterized by low gamma, low

Fig. 1. Stratigraphic column of the Songliao Basin (modified after Wang and Chen, 2015).
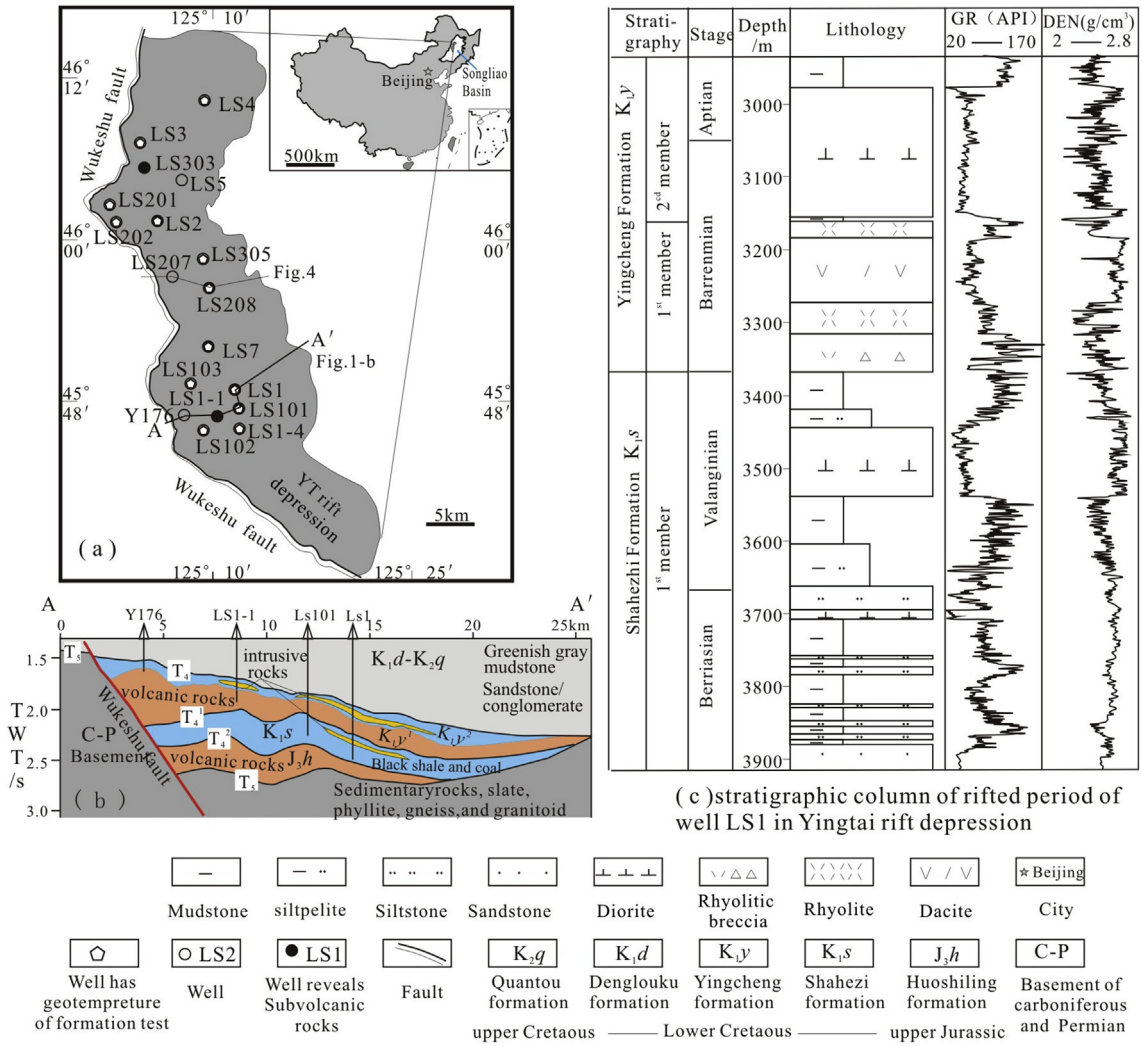
Fig. 2. (a) Location map of the Yingtai rift depression in the Songliao basin, NE China; (b) Cross section drawn across A-A'; (c) Stratigraphic column of the Yingtai rift depression.

acoustic time, high density, and high resistance (Fig. 3). The gamma, acoustic time, and resistance logging curves include medium–high blocky and medium jagged patterns, and the density curve shows a medium blocky, jagged pattern. The seismic facies of the gabbro–porphyrite has a sheet-like-mound shape, with good reflector continuity, medium–strong amplitude, and medium–high frequency (Fig. 5a), similar to the characteristics of laccoliths and sills.

4.2. 2Gas pool

The gas pool is considered to be a lithologic pool of low abundance, high temperature, and normal pressure that is methane rich based on an integrated analysis using coring, logging, seismic imagery, and oil tests (Table 1; Figs. 3 and 5). The gas pool temperature and casing pressure were found to be 149.5 °C and 5.67 MPa, respectively. Experiments on five samples showed that the gas component was mostly CH_4 (91.40%–93.67%) with a minor C_2H_6 component (3.22%–3.50%). The gabbro–porphyrite emplaced within a mudstone or silty pelite unit (Fig. 3b) acts as both the source and cap rock, suggesting that the gas migrated only for a short distance (Fig. 5b).

5. Reservoir characteristics

5.1. Types of void spaces

The intrusive rocks show primary and secondary porosity, such as shrinkage fractures (SF), spongy pores (SP), secondary sieve pores (SSP), and tectonic fractures (TF) (Fig. 6). The shrinkage fractures are irregularly shaped, 1–10 mm wide and 10–30 mm long, and are filled with 30%–95% bitumen and calcite. They are mainly distributed within the middle–upper section of the core (Figs. 6 and 7b). The tectonic fractures comprise regularly spaced vertical fractures that are ~1 mm wide and over 3 m long, along which the core disintegrates. The distance between fractures is 2–4 cm, with either the presence of a low degree of fracture fill or the absence of fracture filling. Spongy and secondary sieve pores are visible in thin sections as light blue to blue irregular and crumbly blocks with indistinct edges and diameters of 50–100 μm. These characteristics suggest that the SSP and SP are poorly developed and that most of the void spaces occur in fractures.

5.2. Porosity and permeability characteristics

The intrusive rock reservoirs have low porosity (0.75%–3.84%) and low permeability (0.003–0.513 mD) (Fig. 6; Table 3). The pore-
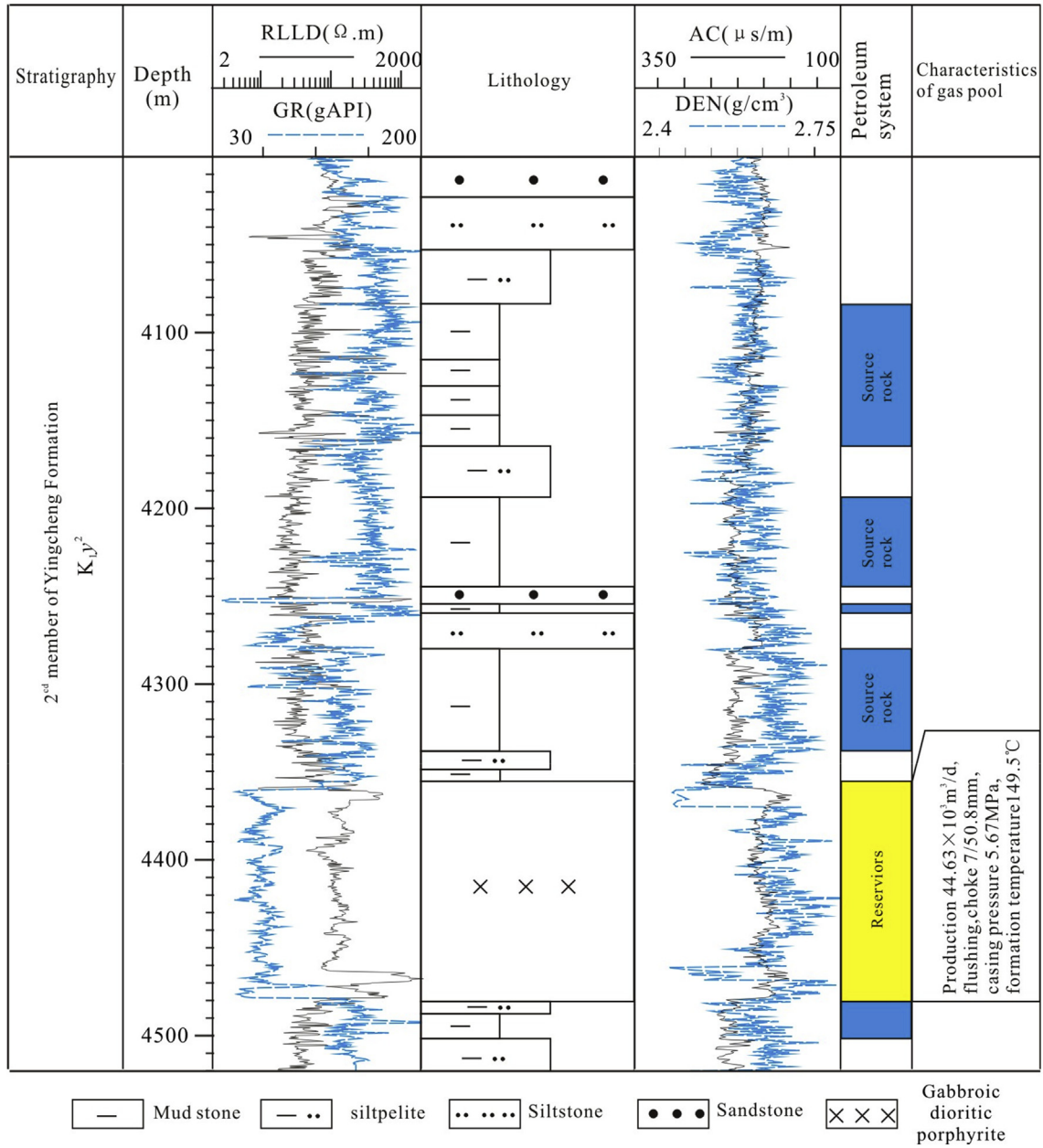
Fig. 3. Stratigraphic column of the Yingtai rift depression intersected/penetrated by well LS208 in Songliao basin, NE China.

Table 2
Characteristics of samples and porosity of intrusive rocks of the 2nd member of the Yingcheng Formation (K_1y^2) from well LS208 in the Yingtai rift depression in the Songliao basin, NE China.

No.	depth	length (mm)	Diameter (mm)	void space	Φ(%)	K (mD)	No.	depth	length (mm)	Diameter (mm)	void space	Φ(%)	K (mD)
1	4422.12	38.66	25.26	SP + SSP	1.202	0.004	11	4425.20	37.53	25.25	SP + SSP	0.747	0.004
2	4422.42	36.84	25.25	SP + SSP	1.173	0.004	12	4425.78	32.73	25.25	SSP + SP	1.220	0.008
3	4422.52	35.23	25.24	SF + SP + SSP	1.935	0.141	13	4425.97	37.48	25.30	TF + SSP + SP	2.051	0.009
4	4423.00	33.19	25.26	SP + SSP	1.624	0.007	14	4426.10	36.18	25.25	SP + SSP	0.972	0.005
5	4423.05	41.58	25.25	SP + SSP	1.195	0.003	15	4426.25	40.50	25.25	SSP + SP	1.348	0.007
6	4423.69	35.08	25.23	SF + SP + SSP	1.684	0.205	16	4426.65	41.73	25.25	SP + SSP	1.011	0.005
7	4423.79	37.41	25.24	TF + SSP + SP	3.000	0.513	17	4426.90	38.22	25.26	SF + SSP + SP	2.274	0.009
8	4424.95	33.01	25.25	SSP + SP	1.848	0.003	18	4427.70	33.78	25.24	TF + SSP + SP	3.843	0.075
9	4425.07	34.22	25.25	SF + SSP + SP	1.992	0.004	19	4428.00	35.62	25.24	SF + SSP + SP	3.560	0.003
10	4425.17	32.63	25.26	SP + SSP	0.820	0.006	20	4428.05	37.55	25.24	SSP + SP	1.721	0.004

Notes: SP-spongy pore, SSP-secondary sieve pore, SF-shrinkage fracture, TF- tectonic fracture.
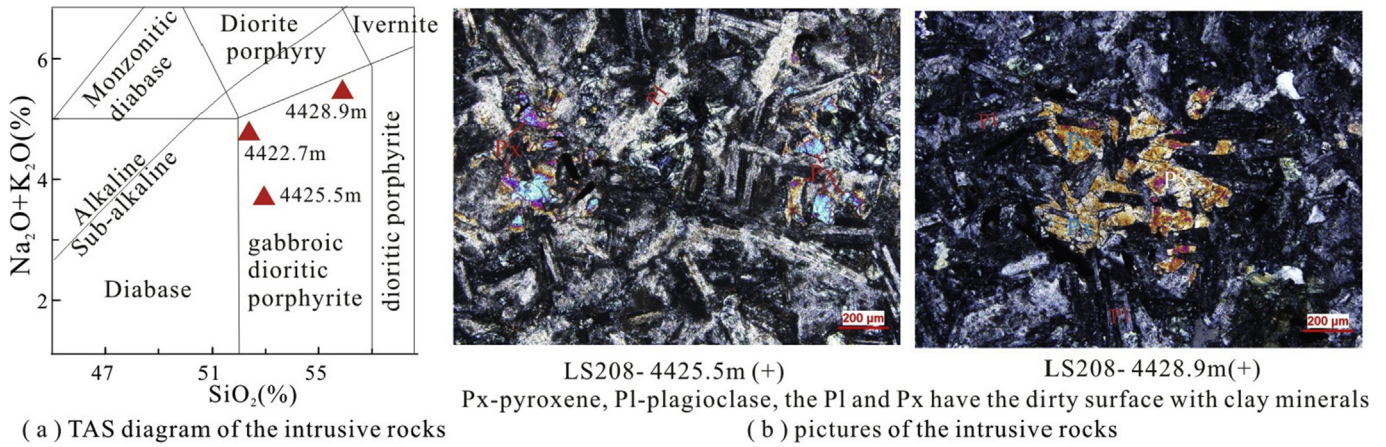
Fig. 4. Characteristics of intrusive rocks from the 2nd member of the Yingcheng Formation observed in well LS208 of Yingtai rift depression in Songliao basin, NE China.
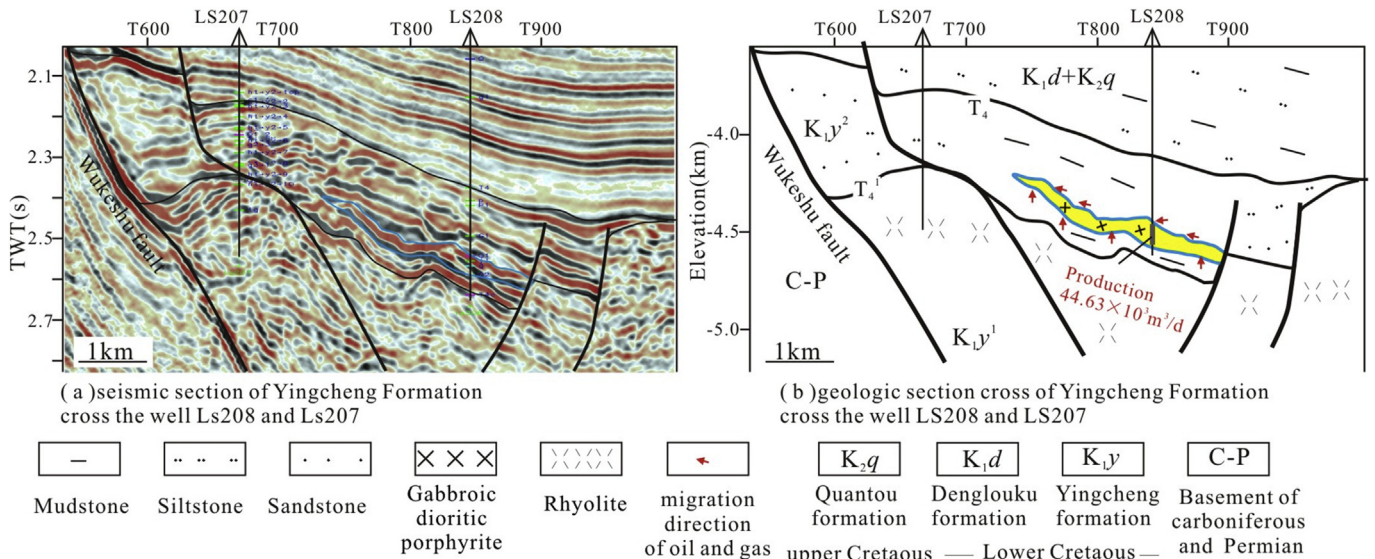

Fig. 5. Geological and Geophysical Characteristics of gas pool of intrusive rocks of the 2nd member of the Yingcheng Formation from well LS208 of the Yingtai rift depression in the Songliao basin, NE China.

throat sizes have an average radius of 0.010–0.028 μm, negative skewness of slanting degree ranging from −1 to 0.012, middle–high displacement pressure ranging from 6.87 to 30.99 MPa, and low saturation during mercury injection (from 39.01% to 75.06%) (Fig. 4).

5.3. Characteristics of void space combinations

Void space combinations in the intrusive rock reservoirs are of three types: TF + SP + SSP (medium–high porosity and high permeability), SF + SSP + SP (medium–high porosity and medium–low permeability), and SSP + SP (medium–low porosity and medium–low permeability) (Table 2; Fig. 8). All the intrusive rock samples comprise SSP + SP, and the porosity contribution obtained from fractures is estimated using the average difference between SSP + SP and TF/(SF + SP + SSP). The 8 samples comprising TF + SP + SSP and SF + SSP + SP have an average porosity of 2.54%. The 12 samples comprising SSP + SP have an average porosity of 1.24%. The average fracture porosity is ~1.30%, and its average contribution to the total porosity is up to 51.2%. However, this does not take into account the fractures that were excluded during

sample preparation, and the true porosity contribution from fractures is likely more than 51.2%. As a result, the intrusive rock reservoirs are of the fracture–pore type.

6. Discussion

6.1. Reservoir formation

Multiple processes affected the gabbro–porphyry intrusive rock during its contact with the country rock. The two major processes involved were (1) a period of cooling and the formation of fractures and joints. These were mainly concentrated along the interface of the intrusive–host rock, at the junction of both the dykes and sills, and at the base of curving sills (Senger et al., 2015); and (2) a post-cooling period that included hydrothermal alteration, precipitation, weathering, and tectonic deformation (Gu et al., 2002; McPhie et al., 1993; Wu et al., 2006). Hydrothermal alteration, weathering, and tectonic deformation most likely increased the total porosity (McPhie et al., 1993; Poursoltani and Gibling, 2011; Hou et al., 2012; Huang et al., 2012; Zou et al., 2011), whereas precipitation reduced both porosity and permeability (Dobson et al.,
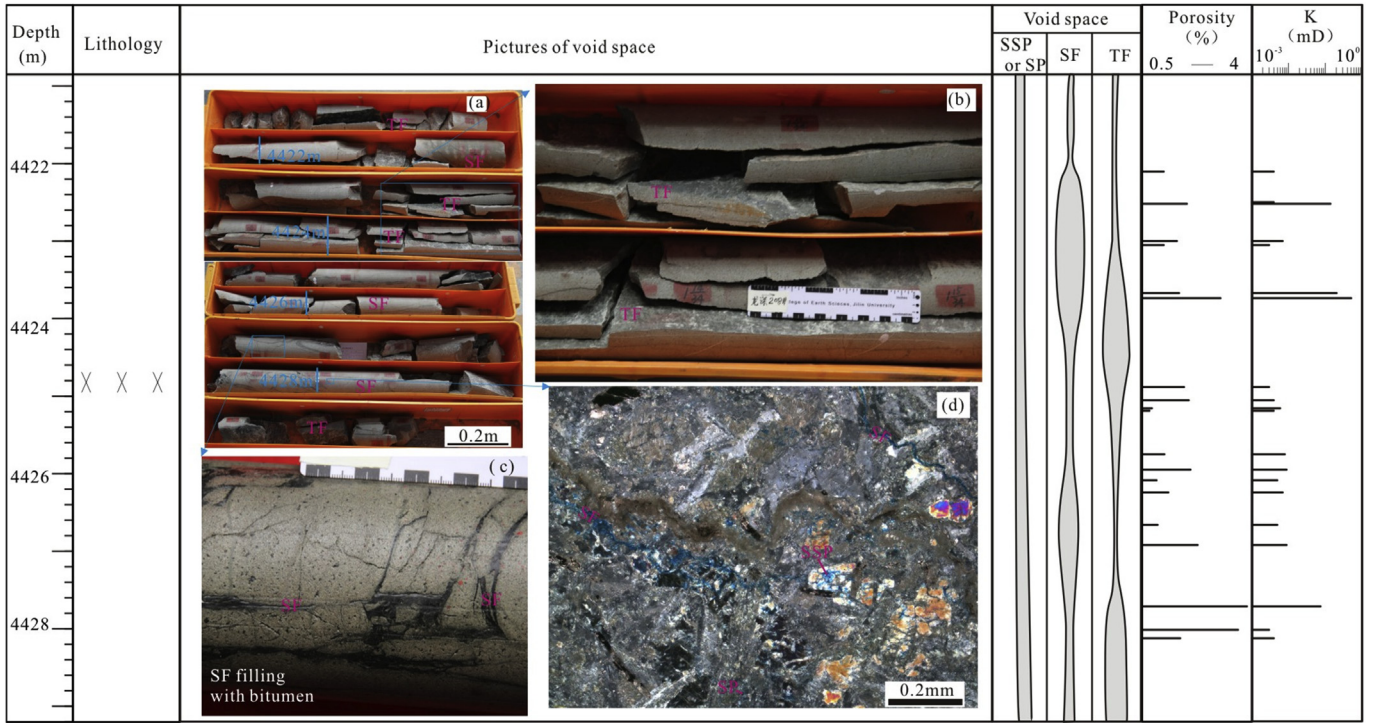
Fig. 6. Reservoir characteristics of intrusive rocks of the 2nd member of the Yingcheng Formation from well LS208 of the Yingtai rift depression in the Songliao basin, NE China. Notes: SS-spongy pore, SSP-secondary sieve pore, SF-shrinkage fracture, TF- tectonic fracture; the lithological mark (see Fig. 3).
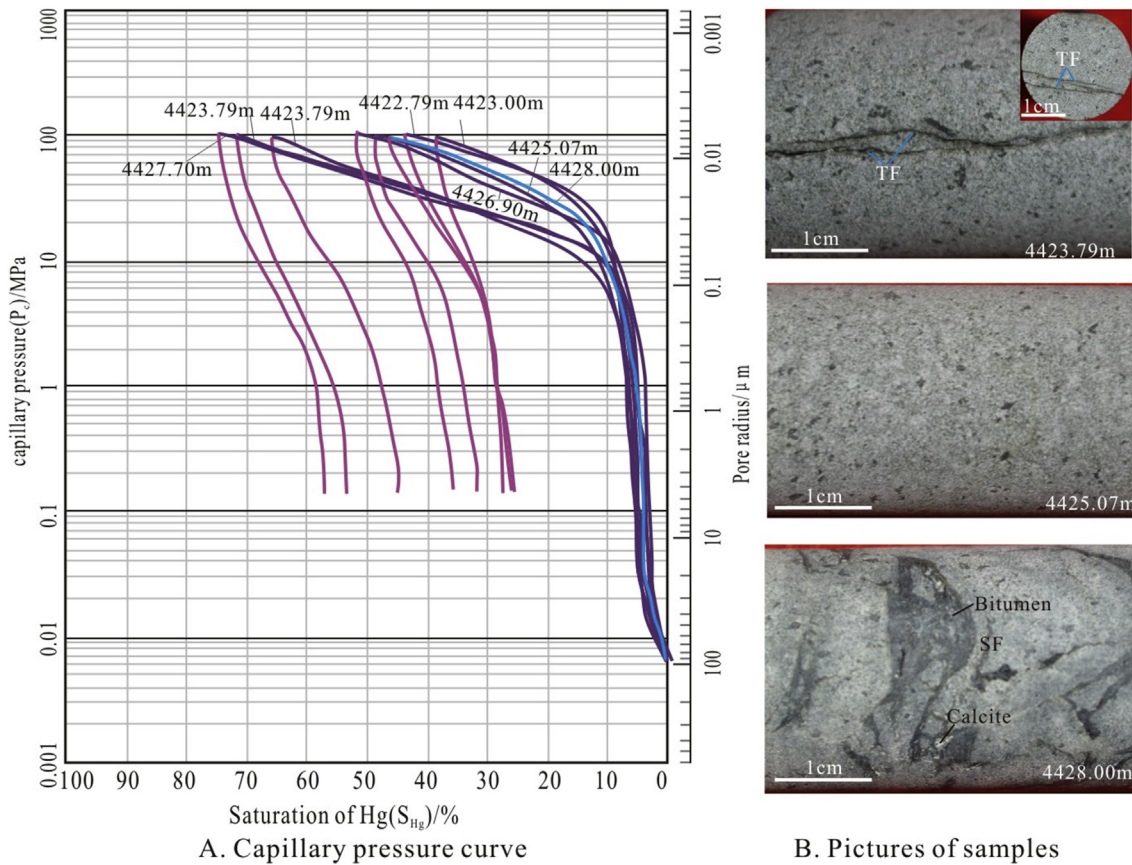

Fig. 7. Capillary pressure curve and sample characteristics of intrusive rocks of the 2nd member of the Yingcheng Formation from well LS208 of Yingtai rift depression in Songliao basin, NE China.

Table 3
Pore throat characteristics of intrusive rocks of the 2nd member of the Yingcheng Formation (K_1y^2) from well LS208 in the Yingtai rift depression in the Songliao basin, NE China.

Depth(m)	K (mD)	φ (%)	Ra (μm)	Rp (μm)	S_p	S_{kp}	Dm (μm)	Φ_p	D_R	$1/D\varphi$	α	Smax (%)	Sr (%)	Pcd (MPa)
4422.52	0.141	1.935	0.071	0.024	1.512	0.024	0.023	0.251	66.428	0.060	0.343	71.477	53.052	10.323
4422.72	0.141	1.935	0.024	0.010	0.908	−1.000	0.009	0.197	105.897	0.048	0.421	43.285	26.112	30.994
4423.00	0.007	1.624	0.024	0.009	0.915	−1.000	0.009	0.030	105.494	0.320	0.392	39.011	27.747	30.992
4423.79	0.513	3.000	0.107	0.027	1.677	−0.359	0.025	0.005	66.125	2.867	0.250	65.670	44.429	6.871
4425.07	0.004	1.992	0.030	0.011	1.095	−1.000	0.011	0.046	99.020	0.218	0.370	48.397	31.307	24.108
4426.90	0.009	2.274	0.043	0.017	1.239	−0.486	0.014	0.040	89.320	0.278	0.398	51.835	35.549	17.229
4427.70	0.075	3.843	0.107	0.028	1.624	0.012	0.025	0.234	64.444	0.066	0.260	75.058	57.193	6.891
4428.00	0.003	3.560	0.030	0.011	1.077	−1.000	0.011	0.019	100.903	0.520	0.373	45.888	25.391	24.115

a.4423.79 m, pore types combination of TF+SP+SSP   b. 4428.00 m, pore types combination of SF+SP+SSP
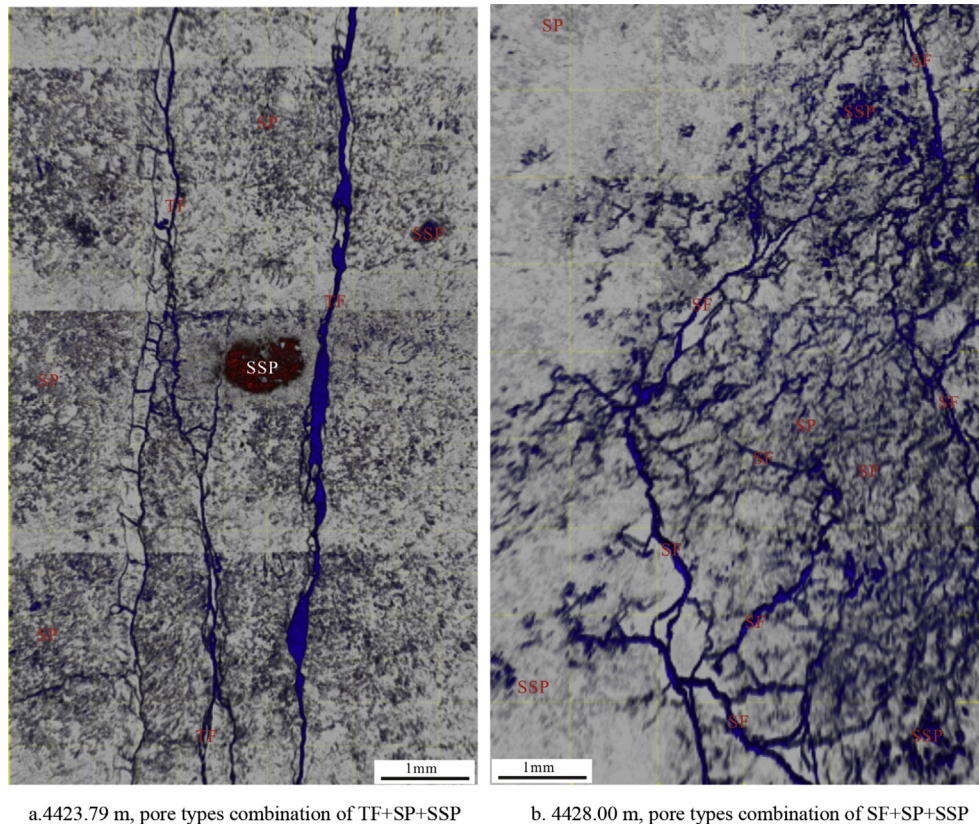
Fig. 8. Pore images of intrusive rocks from well LS208 captured with a laser confocal scanning microscope. Note: TF- tectonic fracture, the regular line with blue color; SF-shrinkage fracture, the netlike line with blue color; SP-spongy pore, the cloudy block with gray color; SSP-secondary sieve pore, the irregular crumbly block with red or blue color. (For interpretation of the references to colour in this figure legend, the reader is referred to the web version of this article.)

2003). The drillcore samples showed evidence of tectonic deformation, cooling shrinkage, and alteration (Fig. 6).

6.1.1. Cooling

Shrinkage fractures occur at the contact between magma and country rock, where thermal stresses associated with cooling generate a network of interconnected polyhedric-curviplanar fractures (Senger et al., 2015; Wu et al., 2006) (Fig. 8b). In terms of the burial history curve, shrinkage fractures formed during the emplacement period (Fig. 9) were later enhanced by the burial processes. Both the bottom and uppermost layers of the intrusion are characterized by a low-resistivity zone that may represent the cooling crust (Fig. 11a). The fractures generated during the cooling period experienced the filling effect and became filled with minerals such as quartz and calcite, which developed gas-liquid two-phase hydrocarbon inclusions (Fig. 9). According to the 36

homogenization temperatures, three peak temperature areas are identified; 130–135 °C, 140–145 °C, and 155–160 °C (Fig. 10). By comparing these to the burial history, the formation time of inclusions was found to be between late Cenomian to Turonian, which is later than the formation of the fractures. Therefore, these fractures were mainly formed during the cooling stage.

6.1.2. Tectonic reworking

The tectonic fractures were formed by tectonic activities that generated interconnected planar fractures (Fig. 8a). An FMI (Formation MicroScanner Image) shows that the tectonic fractures dip to the SSE (Fig. 11b and c), similar to the orientation observed in inverted structures formed during the Middle–Late Campanian (Zhang et al., 1996). In relation to the burial history curve (Fig. 8), the intrusive rock reservoir underwent reverse tectonic activity during the Middle–Late Campanian, which possibly was
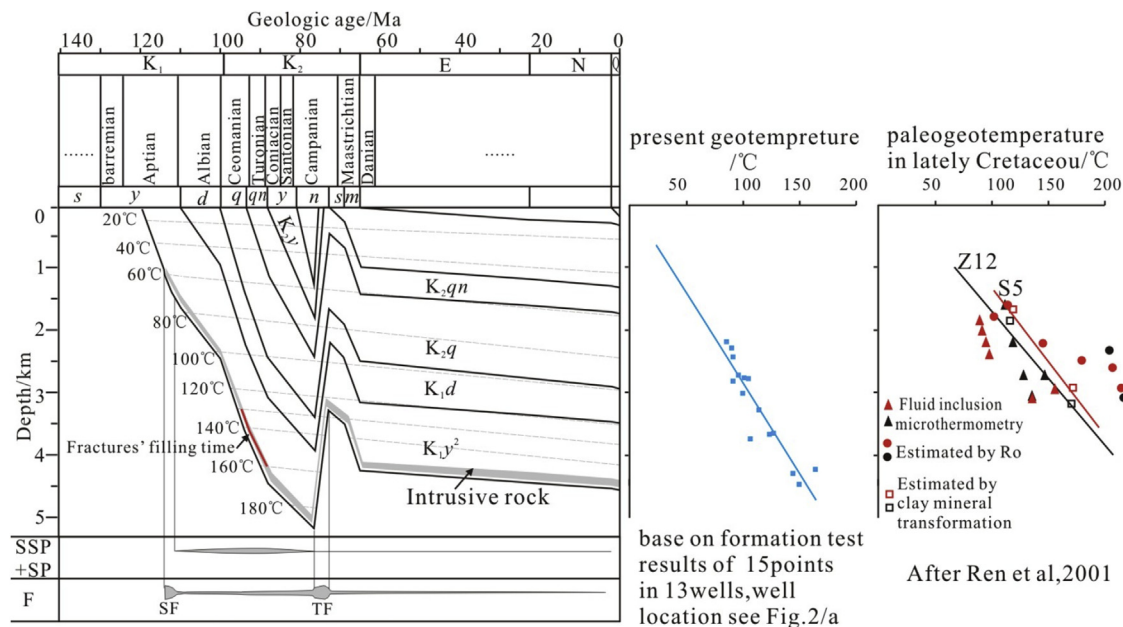
Fig. 9. Burial history curve of intrusive rocks of the 2nd member of Yingcheng formation in well LS208 of the Yingtai rift depression in the Songliao basin, NE China. The geotemperature of formation is determined by formation test results of 15 points in 13 wells. The paleogeotemperature in the late Cretaceous is determined by well Z12 and well S5 with Fluid Inclusion microthermometry data and clay mineral transformation data (Ren et al., 2001). The consolidation of sedimentary stratigraphy is estimated by using normal consolidation lines (Allen and Allen, 2013). The consolidation of intrusive rocks is not estimated.
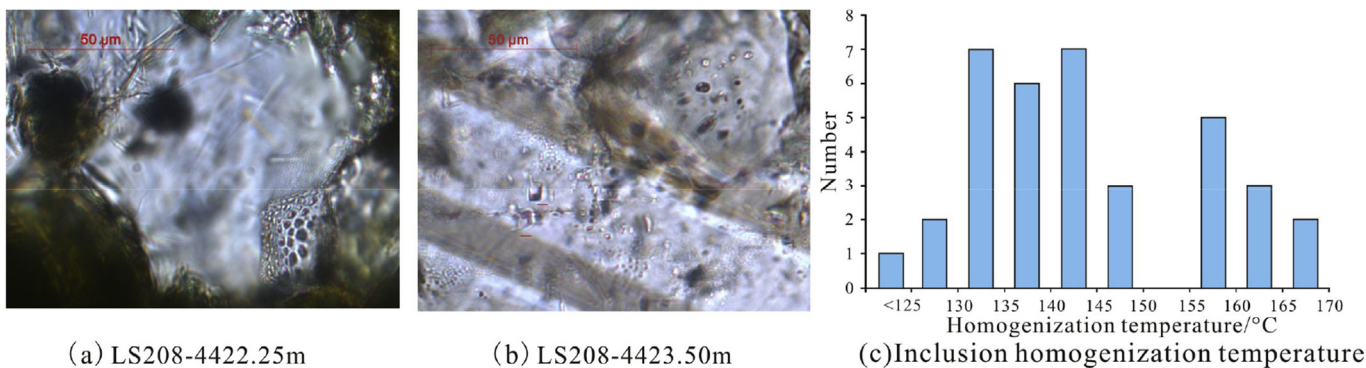

Fig. 10. Characteristics and homogenization temperature of LS208 inclusions of the Yingtai rift depression in the Songliao basin, NE China. The inclusions in picture (a) are distributed in Quartz, while the inclusions in picture (b) are distributed in Calcite.

responsible for the development of tectonic fractures.

6.1.3. Alteration

Mineral alteration involved the replacement of primary minerals and the precipitation of secondary minerals in void spaces between the Albian to Campanian. During this process, the porosity ranged from small to large medium-sized spongy pores and cavernous voids. The alteration of the matrix and minerals, such as plagioclase and pyroxene, generated both secondary pores and secondary sieve pores (Figs. 6d and 8). The total organic content (TOC) of mudstones in the 2nd member of the Yingcheng Formation ranges from 1.1% to 4.3%, and vitrinite reflectance (Ro) ranges from 1.2% to 1.9%. The kerogen is type II. Based on the known maturation process for organic matter in the Songliao Basin, organic acid is generated mainly at temperatures between 70 and 130 °C, while CO_2 is generated mainly between 130 and 170 °C (Chen et al., 1996). In terms of the burial history (Fig. 9), secondary pores and secondary sieve pores formed during the emplacement of the intrusive rock in the late Albian, when the intrusive rocks underwent alteration and dissolution by organic acids and between the early Cenomanian and middle Campanian, when the intrusive rocks underwent alteration and dissolution by carbonic acid.

6.2. Relationship between the reservoir formation and gas accumulation

The intrusive rocks consist of SF, SP, SSP, and TF. In the late Aptian to early Albian, the SFs became charged with oil and gas, due to their abundance and small size. This possibly explains why the SF are filled with bitumen, and with increasing burial depth during the Santonian, the organic matter produced gas. The SSP + SP became charged with gas because of their abundance and larger sizes as a result of the carbonic acid. This process must have continued to have an effect into the middle—late Campanian when the intrusive rocks reached their maximum burial depth. During tectonic inversion and uplift in the middle—late Campanian, the TF became
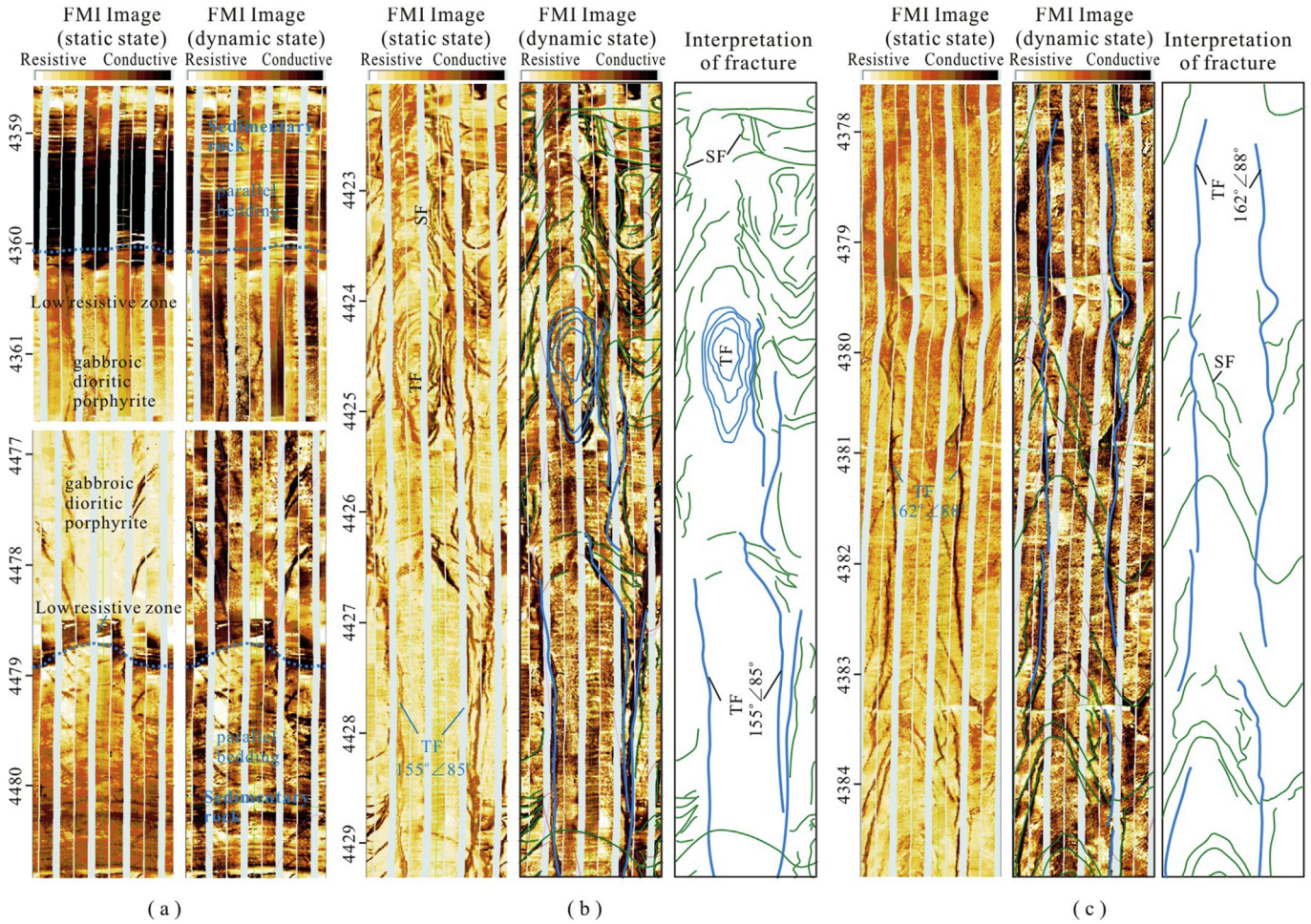
Fig. 11. The FMI characteristics of intrusive rocks and fracture interpretation of the 2nd member of the Yingcheng Formation from well LS208 in the Yingtai rift depression in the Songliao basin, NE China.

effective in distributing the accumulated gas throughout the reservoir.

6.3. Exploration potential

In a petroleum system, magmatism generally affects the maturity and the timing of the expulsion of source rock, especially if the magma intruded immature source rock (Jones et al., 2007; Kontorovich and Khomenko, 2001; Kus et al., 2005; Othman and Ward, 2002; Volk et al., 2002; Wang et al., 2012). The vertical spacing between the contemporaneous emplaced sills has an important influence on the gas generation potential (Aarnes et al., 2011). Igneous intrusion in a coal bed affects the vitrinite reflectance (Rahman and Rimmer, 2014). In addition, the intrusive rock contributes to the formation of potential reservoirs and traps and to the migration and accumulation of hydrocarbons (Polyansky et al., 2003; Stagpoole and Funnell, 2001; Thomaz-Filho et al., 2008).

The intrusive rocks display the reservoir potential and the accumulations of hydrocarbons in the Songliao Basin. Despite the low porosity and permeability characteristics in the large scale reservoirs, the vertical and lateral distribution of oil and gas pools of Songliao Basin is worthy of exploration, especially at burial depths exceeding 3000 m where clastic reservoirs are generally tight and discontinuous (Cao et al., 2012; Wang and Chen, 2015). Generally, the burial depth of Mesozoic rift basins in eastern China exceeds 3000 m, with intrusive rocks comprising mudstone and coal.

Intrusive rocks in other formations of Songliao Basin or nearby basins have potential for gas exploration. For example, the Shahezi Formation in the Yingtai rift depression (Fig. 2) and the Shahejie Formation in the Liaohe basin (Chen et al., 2011) have several of the key characteristics observed in well LS208 that suggest a working petroleum system.

7. Conclusions

The intrusive rock reservoirs of gas pools of the 2nd member of the Yingcheng Formation, penetrated by well LS208 are suggested to be low-abundance, high-temperature, normal-pressure, methane-rich lithologic pools. The intrusive gabbro—porphyrite rock emplaced within mudstone and silty pelite units is both a source and cap rock. The gas accumulations in the intrusive reservoir rocks suggest a short distance migration from the source rock. The gas temperature and casing pressure was found to be 149.5 °C and 5.67 MPa, respectively.

The intrusive rocks display primary and secondary porosity (i.e., SF, SP, SSP, and TF) that are characteristic features of fractured—pore reservoirs. The data suggest that porosity—permeability is low and the capillary pressure curve for mercury intrusion indicates small pore-throat size, negative skewness, middle—high displacement pressure, and middle—lower mercury saturation. The development of fractures is related to the quenching effects during the emplacement period and to tectonic inversion and uplift during the

late Campanian. Spongy and secondary sieve pores formed mainly in two phases: first, during the emplacement period and later by the alteration process influenced by organic acids in the late Albian; and second, during the alteration and dissolution processes influenced by carbonic acid in the early Cenomanian and middle Campanian.

The secondary fracture formed during the emplacement and prior to the filling with hydrocarbons. The SSP + SP formed during the charging period of oil and gas. The TF formed in the late Campanian and contributed to the distribution and accumulations of gas throughout the reservoir. Intrusive rocks that were emplaced within the coal and/or mudstone in the deep Huoshiling, Shahezi, and Yingcheng Formations in the Songliao Basin could have reservoir origins and oil–gas accumulations similar to those of the gas pools found in well LS208. This suggests that there is good potential for gas exploration in intrusive rocks in the region.

Acknowledgments

References

Aarnes, I., Svensen, H., Polteau, S., Planke, S., 2011. Contact metamorphic devolatilization of shales in the Karoo Basin, South Africa, and the effects of multiple sill intrusions. Chem. Geol. 281 (3–4), 181–194.

Allen, P.A., Allen, J.R., 2013. Basin Analysis: Principles and Application to Petroleum Play Assessment, third ed. Wiley-Blackwell.

Cai, Z.R., Huang, Q.T., Xia, B., Lü, B.F., Liu, Wei.L., Wan, Z.F., 2012. Development features of volcanic rocks of the Yingcheng formation and their relationship with fault structure in the xujiaweizi fault depression, Songliao basin, China. Petroleum Sci. 9 (4), 436–443.

Cao, Y.C., Yuan, G.H., Wang, Y.Z., 2012. Genetic mechanisms of low permeability reservoirs of qingshuihe formation in Beisantai area, junggar basin. Acta Pet. Sin. 33 (5), 758–771 (in Chinese with English abstract).

Chen, Z.L., Wang, G.S., Wang, Y., Qing, C.W., 1996. Diagenesis and porosity evolution of lower cretaceous denglouku formation in southern Songliao basin. J. Jianghan Petroleum Inst. 18 (1), 14–18 (in Chinese with English abstract).

Chen, Z.Y., Qiu, J.T., Wang, P.J., Li, B., Zhang, P.X., Liu, X., Hao, T., Li, G.M., 2011. Relationship between volcanic rocks and hydrocarbon accumulation during dominant period of basin formation in liaohe depression. Acta Sedimentol. Sin. 29 (4), 798–818 (in Chinese with English abstract).

Cukur, D., Horozal, S., Kim, D.C., Lee, G.H., Han, H.C., Kang, M.H., 2010. The distribution and characteristics of the igneous complexes in the northern East China Sea Shelf Basin and their implications for hydrocarbon potential. Mar. Geophys. Res. 31 (4), 299–313.

Dobson, F., Kneafsey, T., Hulen, J., Simmons, A., 2003. Porosity, permeability and fluid flow in the Yellowstone geothermal system, Wyoming. J. Volcanol. Geotherm. Res. 123, 313–324.

Feng, Z.Q., 2008. Volcanic rocks as prolific gas reservoir: a case study from the Qingshen gas field in the Songliao Basin, NE China. Mar. Petroleum Geol. 25 (4–5), 416–432.

Feng, Z.Q., Jia, C.Z., Xie, X.M., Zhang, S., Feng, Z.H., Timothy, C.A., 2010. Tectonostratigraphic units and stratigraphic sequences of the nonmarine Songliao basin, northeast China. Basin Res. 22 (1), 79–95.

Filho, A.T., Mizusaki, A.M.P., Antonioli, L., 2008. Magmatism and petroleum exploration in the Brazilian Paleozoic basins. Mar. Petroleum Geol. 25 (2), 143–151.

Gao, Y.F., Liu, W.Z., Ji, X.Y., 2007. Diagenesis types and features of volcanic rocks and its impact on porosity and permeability in Yingcheng Formation, Songliao Basin. J. Jilin Univ. Earth Sci. Ed. 37 (6), 1251–1258 (in Chinese with English abstract).

Ge, R.F., Zhang, Q.L., Wang, L.S., Chen, J., Xie, G.A., Wang, X.Y., 2012. Late Mesozoic rift evolution and crustal extension in the central Songliao Basin, northeastern China: constraints from cross-section restoration and implications for lithospheric thinning. Int. Geol. Rev. 54 (2), 183–207.

Gu, L.X., Ren, Z.W., Wu, C.Z., Zhao, M., Qiu, J., 2002. Hydrocarbon reservoirs in a trachyte porphyry intrusion in the Eastern depression of the Liaohe basin, northeast China. AAPG Bull. 86 (10), 1821–1832.

Guo, R., Zhang, G.C., Zhang, J.W., Zhao, X.B., Liu, J.B., Yuan, D.W., Song, S., 2013. Fingered intrusion of shallow saucer-shaped igneous sills: insights from the jiaojiang sag, east China Sea. Acta Geol. Sin. Ed. 87 (5), 1306–1318.

Hou, L.H., Zou, C.N., Liu, L., Wen, B.H., Wu, X.Z., Wei, Y.Z., Mao, Z.G., 2012. Geologic essential elements for hydrocarbon accumulation within Carboniferous volcanic weathered crusts in Northern Xinjiang, China. Acta Pet. Sin. 33 (4), 533–540 (in Chinese).

Huang, Z.L., Liu, B., Luo, Q.S., Wu, H.Z., Ma, J., Chen, X., Chen, J.Q., 2012. Main controlling factors and models of Carboniferous volcanic hydrocarbon accumulation in the Malang Sag, Santang basin. Acta Geol. Sin. 86 (8), 1210–1216 (in Chinese).

Jia, C.Z., Zhao, W.Z., Zou, C.N., Feng, Z.Q., Yuan, X.J., Chi, Y.L., Tao, S.Z., Xue, S.H., 2007. Geological theory and exploration technology for lithostratigraphic hydrocarbon reservoirs. Petroleum Explor. Dev. 34 (3), 257–272 (in Chinese with English abstract).

Jones, S.F., Wielens, H., Williamson, M.C., Zentilli, M., 2007. Impact of magmatism on petroleum systems in the sverdrup basin, canadian arctic islands, Nunavut: a numerical modelling study. J. Petroleum Geol. 30 (3), 237–256.

Kontorovich, A.E., Khomenko, A.V., 2001. Theoretical foundations of predicting the petroleum potential of sedimentary basins with intense manifestation of trap magmatism. Geol. I Geofiz. 42 (11–12), 1764–1773.

Kus, J., Cramer, B., Kocke, F., 2005. Effects of a Cretaceous structural inversion and a postulated high heat flow event on petroleum system of the western Lower Saxony Basin and the charge history of the Apeldorn gas field. Neth. J. Geosciences-Geologie En Mijnbouw 84 (1), 3–24.

Liu, J.Q., Meng, F.C., Cui, Y., Zhang, Y.T., 2010a. Discussion on the formation mechanism of volcanic oil and gas reservoirs. Acta Petrol. Sin. 26 (1), 1–13 (in Chinese with English abstract).

Liu, W.Z., Huang, Y.L., Pang, Y.M., Wang, P.J., 2010b. Diagenesis of intermediate and mafic volcanic rocks of Yingcheng formation(k1y) in the Songliao basin: sequential crystallization, amygdule filling and reservoir effect. Acta Petrol. Sin. 26 (1), 158–164 (in Chinese with English abstract).

McPhie, J., Doyle, M., Allen, R., 1993. Volcanic Textures: a Guide to the Interpretation of Textures in Volcanic Rocks. University of Tasmania, Tasmania, 196.

Othman, R., Ward, Colin R., 2002. Thermal maturation pattern in the southern Bowen, northern Gunnedah and surat basins, northern new south Wales, Australia. Int. J. Coal Geol. 51 (3), 145–167.

Polyansky, O.P., Reverdatto, V.V., Khomenko, A.V., Kuznetsova, E.N., 2003. Modeling of fluid flow and heat transfer induced by basaltic near-surface magmatism in the Lena-Tunguska petroleum basin (Eastern Siberia, Russia). J. Geochem. Explor. 78–79, 687–692.

Poursoltani, M.R., Gibling, M.R., 2011. Composition, porosity, and reservoir potential of the middle jurassic kashafrud formation, northeast Iran. Mar. Petroleum Geol. 28, 1094–1110.

Rahman, M.W., Rimmer, S.M., 2014. Effects of rapid thermal alteration on coal: geochemical and petrographic signatures in the Springfield (No.5) Coal, Illinois Basin. Int. J. Coal Geol. 131, 214–226.

Ren, Z.L., Xiao, D.M., Chi, Y.L., 2001. Restoration of the palaeogeotherm in Songliao basin. Petroleum Geol. Oilf. Dev. Daqing 20 (1), 13–15 (in Chinese with English abstract).

Rodriguez, F.M., Villar, H.J., Baudino, R., Delpino, D., Zencich, S., 2009. Modeling an atypical petroleum system: a case study of hydrocarbon generation, migration and accumulation related to igneous intrusions in the Neuquen Basin, Argentina. Mar. Petroleum Geol. 26 (4), 590–605.

Senger, K., Buckley, S.J., Chevallier, L., Fagereng, Å., Galland, O., Kurz, T.H., Ogata, K., Planke, S., Tveranger, J., 2015. Fracturing of doleritic intrusions and associated contact zones:Implications for fluid flow in volcanic basins. J. Afr. Earth Sci. 102, 70–85.

Sruoga, P., Rubinstein, N., 2007. Processes controlling porosity and permeability in volcanic reservoirs from the Austral and Neuque'n basins, Argentina. AAPG Bull. 91 (1), 115–129.

Sruoga, P., Rubinstein, N., Hinterwimmer, G., 2004. 2004. Porosity and permeability in volcanic rocks: a case study on the Serie Tob¦fera, South Patagonia, Argentina. J. Volcanol. Geotherm. Res. 132, 31–43.

Stagpoole, V., Funnell, R., 2001. Arc magmatism and hydrocarbon generation in the northern Taranaki basin, New Zealand. Pet. Geosci. 7, 255–267.

Tang, H.F., Li, R.L., Wu, Y.H., Feng, X.H., Wang, L.Y., 2011. Textural characteristics of volcanic strata and its constraint to impedance inversion. Chin. J. Geophys. 54 (2), 620–627 (in Chinese with English abstract).

Tang, H.F., Cryton, P., Gao, Y.F., Huang, Y.L., Bian, W.H., 2015. Types and characteristics of volcanostratigraphic boundaries and their oil-gas reservoir significance. Acta Geol. Sin. Ed. 89 (1), 163–174.

Volk, H., Horsfield, B., Mann, U., Suchy, V., 2002. Variability of petroleum inclusions in vein, fossil and vug cements—a geochemical study in the Barrandian Basin (Lower Palaeozoic, Czech Republic). Org. Geochem. 33 (12), 1319–1341.

Wang, P.J., Chen, S.M., 2015. Cretaceous volcanic reservoirs and their exploration in the Songliao Basin, northeast China. AAPG 99 (3), 499–523.

Wang, K., Lu, X.C., Chen, M., Ma, Y.M., Liu, K.Y., Liu, L.Q., Li, X.Z., Hu, W.X., 2012. Numerical modelling of the hydrocarbon generation of Tertiary source rocks intruded by doleritic sills in the Zhanhua depression, Bohai Bay Basin, China. Basin Res. 24 (2), 234–247.

Wang, P.J., Du, X.D., Wang, J., Wang, D.P., 1995. Chronostratigraphy and stratigraphic classification of the Cretaceous of Songliao basin. Acta Geol. Sin. Ed. 69 (4), 372–381 (in Chinese with English abstract).

Wang, P.J., Chi, Y.L., Liu, W.Z., Chen, R.H., Shan, X.L., Ren, Y.G., 2003. Volcanic facies of the Songliao Basin: classification, characteristics and reservoir significance. J. Jilin Univ. (Earth Sci. Ed. 33 (4), 449–456 (in Chinese with English abstract).

Wang, P.J., Xie, X.A., Frank, M., Ren, Y.G., Zhu, D.F., Sun, X.M., 2007. The Cretaceous

Songliao basin:Volcanogeic succession, sedimentary sequence and tectonic evolution, NE China. Acta Geol. Sin. Ed. 81 (6), 1002—1011.

Wang, J.H., Jin, J.Q., Zhu, R.K., 2011a. Characters and distribution patterns of effective reservoirs in the Carboniferous volcanic weathering crust in Northern Xinjiang. Acta Pet. Sin. 32 (5), 757—766 (in Chinese).

Wang, P.J., Zhang, G.C., Meng, Q.A., Lu, B.L., Zhu, D.F., Sun, X.M., 2011b. Applications of seismic volcanostratigraphy to the volcanic rifted basins of China. Chin. J. Geophys. 54 (2), 597—610 (in Chinese with English abstract).

Wu, C.Z., Gu, L.X., Ren, Z.W., Zhao, M., Zhang, G.H., 2003. Subvolcanic trachyte porphyry at Oulituozi in the Liaohe Basin and its mechanism for hydrocarbon reservoir formation. Geol. Rev. 49 (2), 162—167 (in Chinese with English abstract).

Wu, C.Z., Gu, L.X., Zhang, Z.Z., Ren, Z.W., Chen, Z.Y., Li, W.Q., 2006. Formation mechanisms of hydrocarbon reservoirs associated with volcanic and subvolcanic intrusive rocks: examples in Mesozoic—Cenozoic basins of eastern China. AAPG Bull. 90 (1), 137—147.

Yang, B.J., Liu, W.S., Wang, X.C., Li, Q.X., Wang, J.M., Zhao, X.P., Li, R.L., 2005. Geophysical characteristics of Daxinganling gravitational gradient zone in the East China and its geodynamic mechanism. Chin. J. Geophys. 48 (1), 86—97 (in Chinese with English abstract).

Zhang, G.C., Zhu, D.F., Zhou, Z.B., 1996. Extensional and inversion structureal styles of Songliao basin. Petroleum Explor. Dev. 23 (2), 16—20 (in Chinese with English abstract).

Zou, C.N., Hou, L.H., Tao, S.Z., Yuan, R.K., Zhang, X.X., Li, F.H., Pang, Z.L., 2011. Hydrocarbon accumulation mechanism and structure of large-scale volcanic weathering crust of the Carboniferous in Northern Xinjiang, China. Sci.China Earth Sci. 41 (11), 1613—1626 (in Chinese with English abstract).